Journal of Cleaner Production 319 (2021) 128673

Contents lists available at ScienceDirect

Journal of Cleaner Production

journal homepage: www.elsevier.com/locate/jclepro

A sustainable methanol-based solvent exchange method to produce nanocellulose-based ecofriendly lubricants

Claudia Roman [a], Moisés García-Morales [a], María E. Eugenio [b], David Ibarra [b], Raquel Martín-Sampedro [b], Miguel A. Delgado [a,*]

[a] Departamento de Ingeniería Química, Centro de Investigación en Tecnología de Productos y Procesos Químicos (Pro2TecS), Campus de "El Carmen", Universidad de Huelva, 21071, Huelva (Spain)

[b] Forestry Products Department, Forest Research Centre, INIA-CSIC, Ctra de la Coruña Km 7.5, 28040, Madrid (Spain)

ARTICLE INFO

Handling editorCecilia Maria Villas Bôas de Almeida

Keywords:
Sustainability
Cleaner production
Cellulose nanofiber
Oleogel
Lubrication
Solvent exchange method

ABSTRACT

A prospective methodology aimed to develop totally sustainable oleogels with potential application in lubrication is reported. Oleogels were prepared with cellulose nanofibrils from elm pulps in castor oil. Even at a concentration as low as 1.4 wt%, the oleogels showed rheological behaviors similar to a traditional lithium grease used as reference. In that sense, the high thickening power of cellulose nanofibers was remarked. Never-dried bleached and unbleached elm pulps were mechanically treated with PFI mill refiner and microfluidizer. Moreover, as an alternative way of producing cellulose nanofibrils, the never-dried bleached elm pulp was chemically oxidized using 2,2,6,6-tetramethylpiperidine-1-oxyl radical (TEMPO). The three types of nanofibers were characterized and used in the production of oleogels. The great challenge was to remove the high amount of water retained by the nanofibrils during the nanofibrillation treatment before it was incorporated into the vegetable oil-based lubricant. Alternative strategies such as liophilization or drying failed because the nanofibers, with very high specific surface and strong capacity to interact among them by hydrogen bonding, underwent severe aggregation. Instead, the proposed methanol-based solvent exchange method enabled the transfer of the cellulose nanofibrils from the origin hydrogel to the vegetable oil with no detriment of both their aspect ratio and thickening capacity. Chemical considerations are provided with regard to such a solvent-mediated method, which yielded homogeneous and storage-stable oleogels. This work may attract the interest of lubricant manufacturers to produce nanocellulose-based eco-lubricating greases for industrial applications.

1. Introduction

Lubricants play a vital role in the global industrial sector. They are used in many applications which require a reduction in friction and wear between surfaces in motion. Thus, lubricants provide a better performance and extend the operational life of the machinery. In 2019, the global demand for lubricants was reported to be nearly 36.8 million tons (Sönnichsen, 2000), half of which are uncontrollably released into the environment upon their use (Cecilia et al., 2020). Lubricants embrace a wide spectrum of products which are based, essentially, on mineral or synthetic oils as the main constituent, and a number of additives (thickeners, thermal/lubricity properties improvers, antiwear, etc.). These substances may be highly toxic and with very low biodegradability. Thus, the environmental and health authorities have encouraged to seek sustainable alternatives to both mineral or synthetic oils and hazardous additives (Cecilia et al., 2020). Finding solutions to this problem is one of the greatest current challenges.

In order to increase the ecofriendly character of the lubricants, replacing the mineral and synthetic bases with non-edible vegetable oils has been the adopted approach, mostly. Vegetable oils are universally available, abundant, renewable and non-toxic (Mannekote et al., 2017). Among them, castor oil is of particular interest due to its high viscosity, excellent lubricating properties and the presence of the ricinoleic fatty acid that enables hydrogen bond interaction with other substances containing very electronegative atoms (Quinchia et al., 2014). Even so, the major challenge is yet to find adequate eco-thickeners in order to produce semi-solid lubricants, i.e., eco-lubricating greases. In this scenario, previous studies have demonstrated that lignocellulosic materials

* Corresponding author.
E-mail addresses: claudia.roman@diq.uhu.es (C. Roman), moises.garcia@diq.uhu.es (M. García-Morales), mariaeugenia@inia.es (M.E. Eugenio), ibarra.david@inia.es (D. Ibarra), raquel.martin@inia.es (R. Martín-Sampedro), miguel.delgado@diq.uhu.es (M.A. Delgado).

https://doi.org/10.1016/j.jclepro.2021.128673
Received 7 June 2021; Received in revised form 26 July 2021; Accepted 14 August 2021
Available online 16 August 2021

can effectively act as bio-thickening agents in the production of biogreases (Mu et al., 2018; Núñez et al., 2012; Sánchez et al., 2011). However, their low compatibility with vegetable oils yields gel-like dispersions with poor mechanical stability (Núñez et al., 2012). In this sense, some attempts aimed to enhance the mechanical stability and specific properties of such formulations, through chemical modifications of the lignocellulosic materials, can be found. Thus, Martín-Alfonso et al. (2011) studied a strategy based on the ethylation of kraft cellulose pulps; Gallego et al. (2015) and Borrero-López et al. (2020) increased the hydrophobicity of cellulosic pulps and lignin, respectively, by condensation reactions involving diisocyanates derivatives; and Cortés-Triviño et al. (2019) carried out the epoxidation of an alkali lignin with poly (ethylene glycol) diglycidyl ether (PEGDE), among other molecules. Oleogels with potential application in lubrication were obtained in all cases. Even so, the need for hazardous chemicals and tedious chemical synthesis schemes may constitute serious drawbacks regarding their respect for the environment and feasibility of scaling-up, respectively. So far, limited attention has been paid to the much greater potential of the cellulose nanofibers to form oleogels for lubricant applications.

Nanocellulose is generally produced from chemical pulp fibers, which are obtained in ecofriendly and cost-effective industrial processes (Li et al., 2021). Nanocellulose is comprised by cellulose nanocrystals (CNCs) and cellulose nanofibers (CNFs). Cellulose nanocrystals, also known as cellulose nanowhiskers, show rodlike and highly crystalline structures, with sizes in the range of 5–20 nm and lengths between 200 and 500 nm (Rajinipriya et al., 2018). Contrarily, cellulose nanofibers (or cellulose nanofibrils) are fibrillar structures with both amorphous and crystalline regions, with same diameters as CNCs and lengths up to few micrometers (Rajinipriya et al., 2018). It is worth noting that nanocellulose is a renewable, biocompatible and biodegradable nanomaterial with low density, excellent mechanical and rheological properties, in addition to high surface area and tunable surface chemistry, which allows its interaction with other materials in a controlled manner (Nascimento et al., 2018; Isogai and Zhou, 2019; Li et al., 2021). For all these reasons, nanocellulose may be considered a promising candidate as an eco-thickener in lubricant applications. These properties, much better as compared to the native cellulose fiber, are principally affected by the biomass source (plant species, age and growth conditions, and tissue type), the biomass processing (chemical pulping technology) and the nanocellulose isolation process (mechanical and/or chemical processes) (Michelin et al., 2020).

Woody biomass, as the most common feedstock for pulp and paper industry, is the main source for nanocellulose production (Li et al., 2021). Other sources such as agriculture biomass, industrial waste, bacteria, algae and tunicate are also possible (Rajinipriya et al., 2018; Li et al., 2021). Among different woody materials, several species including hardwoods (e.g., eucalyptus, birch and aspen) and softwoods (e.g., spruce, pine and fir) have been widely used to produce cellulose nanofibers (Rajinipriya et al., 2018; Kandhola et al., 2020; Michelin et al., 2020). Recently, elm (*Ulmus minor* Mill.) wood has been successfully assayed for this purpose (Jiménez-López et al., 2020). Its outstanding growth features and excellent adaptation to different environments, from Spain to UK, make it a potential candidate for producing wood products, including nanocellulose (Martín-Sampedro et al., 2019; Jiménez-López et al., 2020).

Regarding the cellulose nanofibrils isolation process, the chemical pulp fibers are submitted to high-shear mechanical treatment by high-pressure homogenizers or microfluidizers which fibrillates them into high aspect ratio nanofibers (Nechyporchuk et al., 2016). In most cases, cellulosic pulp refining using PFI mills or disk refiners is performed prior to microfluidization to reduce energy consumption (Rajinipriya et al., 2018). A more energy-efficient alternative is the use of chemical pretreatments such as TEMPO (2,2,6,6-tetramethylpiperidine-1-oxyl radical)-mediated oxidation (Saito et al., 2006; Nechyporchuk et al., 2016). The final product consists of negatively charged fibrils which, due to electrostatic repulsion, form stable gel-like aqueous suspensions which facilitate further nanofibrillation (Shinoda et al., 2012). TEMPO-mediated oxidation prior to mechanical microfluidization is usually applied on totally bleached chemical pulps, resulting in cellulose nanofibers with only trace amounts of residual lignin and hemicelluloses. Instead, PFI refining prior to mechanical microfluidization can be also used for CNFs production from unbleached chemical pulps, leading to non-oxidized cellulose nanofibers with high lignin and hemicelluloses content (Iglesias et al., 2020). Unbleached chemical pulps offer the advantage of higher yields (referred to carbohydrates amount) and reduced processing costs and environmental impact by avoiding bleaching steps (Iglesias et al., 2020).

Despite the promising properties offered by cellulose nanofibrils, their high water content (they are commonly available as a hydrogel with a solid content of 2–10 wt%) is a key point in their storage, transport and use (Arvidsson et al., 2015). For applications such as pulp and paper, food, paints, coatings, inks, adhesives and those related with biomedical and cosmetic products, cellulose nanofibril hydrogels are used relatively easily (Li et al., 2021). However, the complete water removal from cellulose nanofibers still remains as the biggest challenge when they are subjected to further chemical functionalization or directly incorporated into products with hydrophobic characteristics such as plastics, textiles, lubricants, foams and films (Nascimento et al., 2018; Li et al., 2021). In that sense, to the best of our knowledge, the present research work is probably the very first to report the preparation of cellulose nanofibers-based eco-lubricants aided by a methanol-based solvent exchange method, from cellulose nanofibrils aqueous dispersions with very high water contents. Such a process drastically reduces the use of chemicals and simplifies the lubricant manufacture. The investigation explored the use of three types of cellulose nanofibers from elm cellulosic pulps (two, bleached and unbleached, CNF samples produced by PFI refining prior to mechanical microfluidization; and a bleached CNF sample obtained by chemical TEMPO-mediated oxidation prior to mechanical microfluidization) as eco-thickening agents in castor oil. Moreover, a preliminary rheological characterization of the oleogels is presented, and a comparative analysis with respect to a traditional lithium–based lubricating grease (benchmark) is established.

2. Materials and methods

2.1. Materials

Castor oil, with kinematic viscosity at 40 °C of 242.5 cSt, was selected as base oil. It was supplied by Guinama (Spain). Basic properties and compositional details of castor oil can be found elsewhere (Ogunniyi, 2006; Quinchia et al., 2010).

The *Ulmus minor* clone Ademuz used in this work, is registered in Spain as resistant to Dutch elm disease (DED) (Martín et al., 2015) and it was supplied by Universidad Politécnica de Madrid.

2.2. Cellulose nanofibers production

For the production of cellulose nanofibers, elm chips were first subjected to a standard kraft pulping according to protocol described by Jiménez-López et al. (2020). Then, part of the obtained pulp was submitted to a bleaching process to reduce mainly its lignin content. After obtaining the different pulps, chemical (TEMPO-mediated oxidation) or physical (PFI refining) pretreatments were used over the never-dried pulps, in order to increase the effectiveness of the final microfluidization stage.

On one hand, mechanical pretreatment was carried out over unbleached and bleached pulps, and consisted of a refining step in a standard laboratory PFI mill followed by an extensive mixing using an Ultra-Turrax disperser (T25, IKA) in order to improve fibrillation and prevent clogging of the microfluidizer. On the other hand, bleached pulp was also submitted to a chemical pretreatment (TEMPO-mediated oxidation) following the methodology described previously by other

Table 1
Chemical composition of the cellulose nanofibers studied.

TYPE	GLUCAN (wt.%)	XYLAN (wt.%)	KLASON LIGNIN (wt.%)	AC. SOLUBLE LIGNIN (wt.%)	TOTAL LIGNIN (wt.%)	CARBOX. GROUPS (μmol/g)
CNF–U	80.0 ± 0.6	16.4 ± 0.1	1.5 ± 0.2	1.1 ± 0.1	2.6 ± 0.2	56.2 ± 3.9
CNF–B	82.6 ± 0.1	14.7 ± 0.1	0.8 ± 0.3	0.9 ± 0.0	1.7 ± 0.3	52.7 ± 8.9
CNF-TO	65.4 ± 0.2	10.5 ± 0.1	0.0 ± 0.1	1.2 ± 0.1	1.2 ± 0.1	1178 ± 37

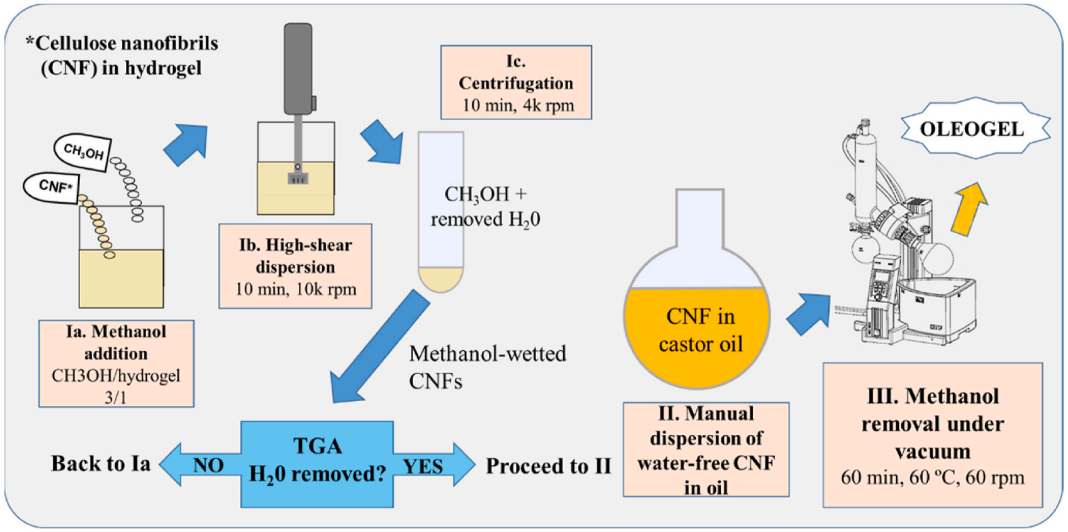

Fig. 1. Schematic illustration of the methanol-based solvent exchange method.

authors (Shinoda et al., 2012), using 0.1 g/g oven-dried pulp (o.d.p.) of NaBr, 0.016 g/g o.d.p. of TEMPO and 10 mmol/g o.d.p of NaClO, at room temperature and pH 10. More details about the pretreatments could be found at Jiménez-López et al. (2020).

Finally, all pretreated fibers suspensions (2 % wt./vol) were submitted to a microfluidization step using a high-pressure fluidizer (Microfluidizer M-110EH, Microfluidics Corp.; Westwood, MA, USA). In the case of refined fibers, the suspension was looped 6 times through a 200 μm interaction chamber and then 7 times adding a 100 μm interaction chamber after the 200 μm one. However, TEMPO-oxidized fibers were passed once through a chamber of 200 μm and then 3 more times using sequential chambers of 200 and 100 μm.

Resulting cellulose nanofibers were stored at 4 °C and identified as CNF–B, CNF–U and CNF-TO for bleached refined, unbleached refined and TEMPO-oxidized nanofibers, respectively.

2.3. Cellulose nanofibers characterization

The chemical composition of CNFs, as determined according to NREL/TP-510-42618 (National Renewable Energy Laboratory, 2011), is gathered in Table 1. A modified conductivity titration method described by Saito and Isogai, 2004), was preferred to determine the carboxylate contents of the cellulose nanofiber samples.

To determine nanofibrillation yield, 0.1% (wt./vol) nanofibers suspensions were centrifuged for 20 min at 4.5k rpm. According to Besbes et al. (2011), the resulting supernatant contents the nanofibrillated fraction while the non or partially fibrillated fibers remain in the sediment. Moreover, the average diameter of fibrils in the nanofibrillated fractions was determined by means of Atomic Force Microscopy (AFM), as previously published in Jiménez-López et al. (2020).

Crystallinity index (CrI) of cellulose nanofibers was measured by X-Ray powder diffraction (XRD) in a Bruker D8 Advance diffractometer (Bruker, Billerica, MA, USA) with Ni filter and Cu anode. Measurements were acquired from 3° to 45° (2θ diffraction angle), using a goniometer speed of 1 s per step and a step size of 0.04. Crystallinity index (CrI) of samples was calculated following the Segal method (Segal et al., 1959).

Water vapor sorption isotherms were studied with a dynamic water vapor sorption equipment (Aquadyne DVS, Quantachrome Instruments) between 0% and 95% relative humidity (RH) at 25 °C. Sorption isotherms were fitted to GAB model (Belbekhouche et al., 2011), that calculates total water uptake (C_{GAB}) as function of water activity ($a_w = RH/100$) according to equation (1):

$$C_{GAB} = C_m \cdot \frac{C_G \cdot K_{ads} \cdot a_w}{(1 - K_{ads} \cdot a_w) \cdot (1 + (C_G - 1) \cdot K_{ads} \cdot a_w)} \quad (1)$$

where: C_m represents the amount of water adsorbed onto the monolayer; K_{ads} is related to the adsorption enthalpy difference between the first layer and the following; and C_G is the Guggenheim constant which estimates the strength of bound water to the primary binding sites.

2.4. Oleogels preparation

Cellulose nanofibers were available as gel-like aqueous suspensions having solid contents of ca. 2 wt%. Water removal and further incorporation of the CNFs into castor oil involved a solvent exchange method using methanol, as graphically detailed in Fig. 1. Methanol was added to the hydrogel weight needed to prepare about 50 g oleogel with the target CNF concentrations, 0.7 and 1.4 wt% (methanol/hydrogel weight ratio of 3/1). Then, a T25 digital Ultra-Turrax homogenizer was used (25 °C, 10 min, and 10k rpm) in order to ensure an intimate mixing between the wet CNFs and the methanol solvent, facilitating the solvent swap. This step was followed by centrifugation (in Thermo Scientific™ Sorvall™ ST 8 Small Benchtop Centrifuge) for 10 min, at 4k rpm, which enabled to separate a methanol-wetted nanocellulose precipitate from a water/methanol supernatant. This stage was repeated until complete water removal from the nanofibers (corroborated by TGA measurements). The number of washes depended on the CNF type. Three washes were enough for non-oxidized nanofibers (CNF–B and CNF–U), whilst four washes were necessary for TEMPO-oxidized nanofibers. Subsequently, the methanol-wetted nanocellulose precipitate was transferred

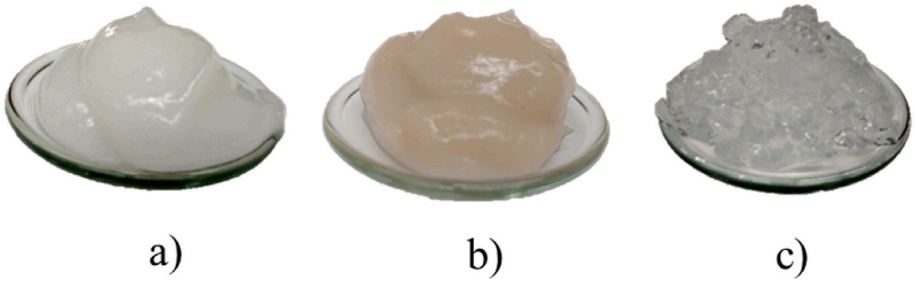

Fig. 2. Photos of the original hydrogels on 50 mm watch glasses: a) bleached PFI refined nanofibers (CNF–B); b) unbleached PFI refined nanofibers (CNF–U); c) TEMPO-oxidized nanofibers (CNF-TO).

into a round flask containing 50 g castor oil and manually dispersed for 10 min. Finally, the mixture was subjected to methanol removal under vacuum (Heidolph Laborota 4001 Rotary Evaporator) for 60 min, at 60 rpm and 60 °C, in order to evaporate all possible solvent remaining. Upon completion of the whole procedure, a homogeneous and storage-stable oleogel was obtained.

2.5. Oleogels characterization

Morphological observations of both hydrogels' and oleogels' microstructures were conducted, at room temperature, with a scanning electron microscope (SEM), model ZEISS EVO LS15 (ZEISS, Germany), at 10 kV. A magnification of 7000 x was used. Previously, all samples were chemically fixed on the holder with 2.5 wt% glutaraldehyde in 0.1 M cacodylate buffer, for 2 h, followed by three washes in 0.1 M cacodylate solution. Subsequently, all samples were subjected to a second fixation with 1 wt% osmium tetraoxide solution, for 1 h, again followed by three washes with 0.1 M cacodylate solution. Finally, all samples were submitted to critical point drying in acetone before being metallized with Au/Pd. Representative morphology prototypes were assured by using, for each formulation studied, at least three different samples and taking five pictures at different locations.

Thermal behavior evaluation was conducted by differential scanning calorimetry (DSC). Measurements were performed with a Q-100 analyzer (TA Instrument, USA), using 5–10 mg samples sealed in hermetic aluminium pans. Cooling and heating rates of 5 °C/min were applied to all samples within a temperature window ranging from −65 up to 200 °C. In order to erase their thermal history, all samples were subjected to an isothermal step at 200 °C for 10 min. DSC was also used to evaluate the oxidation resistance of these oleogels according to ASTM E2009-08 standard. Moreover, in order to monitor the water removal during the oleogel preparation, thermogravimetric analysis (TGA) under inert N_2 atmosphere was carried out with a Q-50 analyzer (TA Instruments, USA). Approximately, 15 mg samples were placed on a Pt pan, and heated from 30 to 120 °C, at 10 °C/min, under N_2 total flow of 50 mL/min. All measurements were replicated at least twice.

Unworked penetration indexes were determined according to the ASTM D1403 standard, using the Seta universal penetrometer, model 17000–2 (Stanhope-Seta, UK), with a one-quarter cone geometry. The one-quarter-scale penetration values were converted into the equivalent full-scale cone penetration values according to ASTM D217. For the sake of comparison, an approximation of NLGI grade was achieved.

The oleogels rheological behavior was analyzed using the controlled-stress rheometer Physica MCR-301 (Anton Paar, Austria), with parallel plate-plate geometry of 25 mm diameter and 1 mm gap, at 25 °C. Steady state viscous flow tests were performed in a shear rate interval ranging from 10^{-2}–10^{2} s^{-1}. Moreover, the linear viscoelastic behavior was also evaluated through dynamic shear frequency sweeps, between 0.08 and 100 rad/s, at strain values within the linear viscoelastic (LVE) range. Preliminary dynamic strain sweep tests, at 1 Hz, were carried out in order to determine the strain range over which the viscoelastic functions were not strain-dependent (LVE range). At least two replicates of each test were conducted on fresh samples.

3. Results and discussion

3.1. A comparative analysis between the different cellulose nanofibers

The characteristics of the CNFs depend mainly on the nanocellulose production process, but also on the properties of the initial pulp from which the CNFs are isolated (Michelin et al., 2020). This work focuses on the feasibility of three types of cellulose nanofibers from elm cellulosic pulps: unbleached (CNF–U) and bleached (CNF–B) cellulose nanofibers produced by PFI refining, and bleached CNF obtained by chemical TEMPO-mediated oxidation (CNF-TO) prior to mechanical microfluidization (Fig. 2). Chemical compositions of the CNFs studied are shown in Table 1. As it was expected, higher lignin and hemicelluloses (xylan) contents were found in CNF–U compared to CNF–B, due to the lack of bleaching process. Furthermore, lower nanofibrillation yield was achieved when unbleached pulp was used (50.2% compared to 60.8% for bleached pulp), indicating a higher proportion of non-fibrillated or partially fibrillated fibrils (microfibrils) in the gel-like suspension obtained after the microfluidization process. This fact could be caused by a more hydrophobic structure in unbleached pulp (due to higher lignin content) which hamper swelling and yield of fibrillation (Solala et al., 2020). Nonetheless, other authors observed an improvement in degree of fibrillation for lignin-containing fibers, because of they may avoid bonds between the cellulosic mechano-radicals formed during microfluidization, resulting in less crosslinked cellulose structure (Rojo et al., 2015; Solala et al., 2020). In this sense, AFM images of the nanofibrillated fractions showed thinner nanofibers in CNF–U sample, with diameter of 3.7 ± 0.7 nm, compared to 5.9 ± 1.7 nm for CNF–B. Longitudinally, larger chain lengths of the bleached nanofibrils were appreciated. Jiménez-López et al., 2020 also observed a more homogeneous length distribution of shorter nanofibers in unbleached CNF.

Regarding the nanocellulose production process, it had a very significant effect on the nanofibrillation yield and carboxylate content. In that sense, the TEMPO-oxidation pretreatment prior to microfluidization selectively converted the C6 primary hydroxyl groups of cellulose to carboxylate groups (Isogai et al., 2011). A carboxylic group content of 1178 μmol/g was obtained for CNF-TO compared to 53–56 μmol/g for CNFs from mechanical pretreatments. This fact provoked electrostatic repulsion between adjacent fibrils which enhanced fibrillation, yielding much thinner nanofibers (diameter of 2.6 ± 0.7 nm) than the non-oxidized nanofibers (CNF–B and CNF–U). Moreover, a 100% nanofibrillation yield was achieved for CNF-TO, indicating the lack of non-fibrillated and microfibrils in this sample, also confirmed by SEM (Fig. 8e). Furthermore, the introduction of –COOH groups caused a significant increase in glucuronic acid (22.9 wt%, compared to 1 and 1.1 wt% in CNF–B and CNF–U, respectively) and a consequent lower glucan percentage (65.4 wt%). According to other authors (Okita et al., 2011; Fillat et al., 2018), the oxidation and/or degradation during chemical pretreatment led to a reduction in hemicelluloses and lignin contents. Finally, no big differences were found in crystallinity index

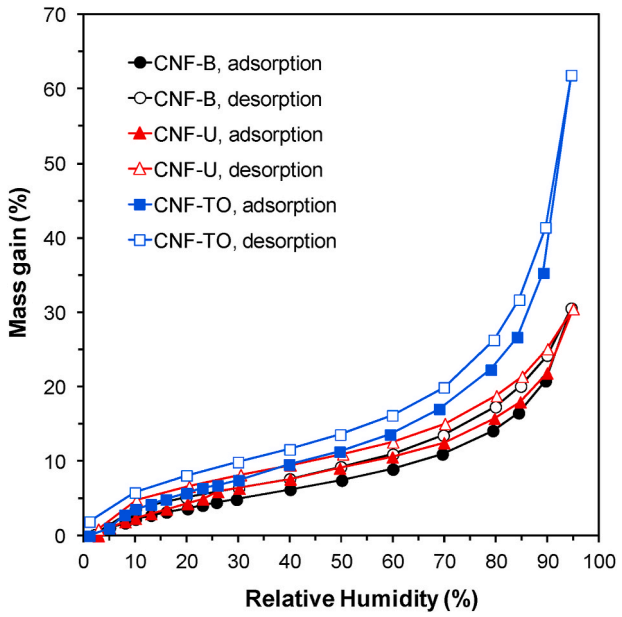

Fig. 3. Water vapor sorption and desorption isotherms of cellulose nanofibers at 25 °C.

Table 2
Sorption parameters of GAB models, determined from water vapor sorption isotherms.

	C_m	C_G	K_{ads}	R^2
CNF–B	4.0	11.9	0.9	0.998
CNF–U	5.2	9.9	0.9	0.998
CNF-TO	5.4	17.2	1.0	0.998

between the three samples: 83.6 ± 0.5%, 85.7 ± 2.5% and 83.5 ± 1.5% for CNF–U, CNF–B and CNF-TO, respectively.

All these properties had effects on the interaction of the nanofibers with water, which is an important factor in the preparation of oleogels. Water vapor sorption tests provided information about the relative hydrophilicity of the three cellulose nanofibers samples studied. Fig. 3 shows their sorption and desorption isotherm curves. Their sigmoid profiles are similar to those of hydrophilic materials (Belbekhouche et al., 2013). These curves were successfully fitted to GAB model (Table 2), which is extensively used for cellulosic materials (Meriçer et al., 2017), showing good accuracies with experimental data (see regression coefficients R^2).

Due to the higher carboxylate content on the surface of CNF-TO, GAB model pointed out stronger bounds between water and primary binding sites (higher C_G). This model also indicated higher amount of water adsorbed onto the monolayer (C_m) in this oxidized sample, probably due to the higher proportion of nanofibers (100% nanofibrillation yield) which provided a higher surface area compared to non-oxidized nanofibers. As far as the nanofibers from mechanical treatment (PFI refining) are concerned, GAB model suggested a weaker interaction between CNF–U surface and water in the monolayer (lower C_G) compared to CNF–B. This is likely caused by the presence of residual lignin. Even so, the higher water adsorption in the monolayer (C_m) observed in CNF–U in comparison with CNF–B was most probably due to the lower diameter of its nanofibrillated fraction and its higher hemicelluloses content.

The higher sorption hysteresis (Fig. 3) observed for CNF-TO, especially at high relative humidities indicates a higher swelling, which also contributes to the large water uptake at high relative humidities: 62% for CNF-TO compared to 28–31% for non-oxidized samples at 95 %RH.

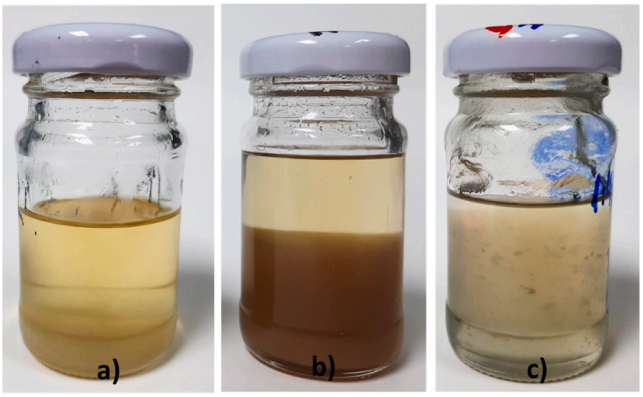

Fig. 4. Phase-separated 1.4 wt% oleogels resulting from the direct incorporation of the water-wetted cellulose nanofibers into castor oil. a) CNF–B; b) CNF–U; c) CNF-TO.

3.2. Enabling homogeneous and storage-stable cellulose nanofibers-based oleogels

Upon fibrillation, the cellulose nanofibers obtained from elm chemical pulps remained in a stable suspension with high water content, ca. 98 wt%, and gel-like texture (Fig. 2). As Chang et al. (2016) pointed out cellulose-water H-bonds formed on the nanocellulose surface weaken the interaction between adjacent cellulose nanofibers, yielding stable nanocellulose hydrocolloids. However, H-bonding handicaps the dispersibility of cellulose nanofibers in a vegetable oil, thereby hampering the preparation of homogeneous and storage-stable cellulose nanofibers oleogels.

Removing water from the fibers without affecting their nano-scale dimension was a tricky challenge. As shown in Fig. 4, phase-separated oleogels resulted when the highly hydrophilic cellulose nanofibers were directly poured into the vegetable oil, even though oleogels were submitted to vacuum rotavaporation at 0.025 bar and 60 °C to eliminate moisture. Cellulose-water H-bond has a higher binding energy than cellulose-ricinoleic acid H-bond (Beck et al., 2012). Hence, the moisture physically attached to individual cellulose nanofibers may effectively prevent the H-bond formation with the ricinoleic fatty acid present in castor oil. Based on that, and given the complete immiscibility of water in oil, the cellulose-water H-bonds formed on the CNFs surface yielded their agglomeration and settling when the water was removed (Chang et al., 2016; Foster et al., 2018).

For this reason, cellulose nanofibers oleogels were prepared by a methanol-based solvent exchange method. The strategy consisted in subjecting the moisture-containing nanofibers to various cycles of methanol wash followed by centrifugation. Intimate contact between methanol and nanofibers was ensured using high shear mixing. Finally, rotavaporation at 0.025 bar and 60 °C was used to eliminate the remaining methanol, yielding stable and homogeneous oleogels. As Wei and Cheng (2007) pointed out, the solvent exchange method has the advantage of degrading less the cellulose nanofibers as compared to other methods. The solvent selection is a key point in such a process. Okura et al. (2014) found out that cellulose nanocrystals and TEMPO (2,2,6,6-tetramethylpiperidine-1-oxyl)-oxidized cellulose nanofibers dispersed well in solvents with dielectric constants greater than 12.9, and viscosities higher than 0.55 cP. In this sense, a number of polar solvents such as acetonitrile, DMSO, DMF, formic acid, ethanol or methanol, to name a few, might be potential candidates. Among them, methanol was chosen because of its lower normal boiling point of 64.7 °C, lower price and lower toxicity. Moreover, cellulose was not solubilized in methanol (El Seoud et al., 2008), thus, no loss of nanocellulose nanofibrils occurred during the solvent exchange process. According to the different water uptake capacity of the nanocelluloses studied (Fig. 3), the CNF–U needed three methanol washes up to

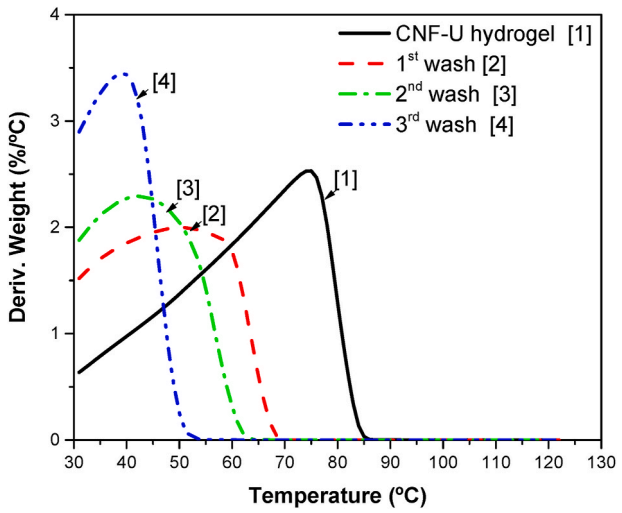

Fig. 5. Derivative weight loss TGA curves for CNF–U samples after every wash with methanol.

complete water removal. Fully compatibilization with castor oil was thus possible. The CNF–B also required three methanol washes, while four methanol washes were necessary in the case of CNF-TO because of its higher water uptake capacity. Thermogravimetric analysis allowed concluding that the derivative weight loss peak progressively increased and shifted to lower temperatures after every methanol wash-centrifugation step, as a consequence of water being replaced by methanol, with higher volatility and lower normal boiling point. This is exemplified in Fig. 5 for the CNF–U only (CNF–B and CNF- TO results are not shown).

Fig. 6 shows the cellulose nanofibers-based oleogels in castor oil, at concentrations of 0.7 and 1.4 wt%, resulting from a methanol-based solvent exchange method. In all cases, homogeneous and stable oleogels were obtained no matter which nanocellulose type was used.

According to Batista da Silva et al. (2011), water molecules have a higher capacity to forming H-bonds between them than methanol. In fact, Benson et al. (2013) pointed out the formation or breakdown of the system-wide H-bonding network at a critical threshold, such that H-bonded water clusters are embedded in loosely coupled methanol molecule structures for water-methanol mixtures with low water content. Thus, the methanol-based washes induced the formation of H-bonded water clusters and the consequence displacement of the water molecules away from the cellulose nanofibers, being sucked into the methanol phase. Moreover, the individual methanol-wetted cellulose nanofibers can effectively prevent the H-bond formation between CNFs (Chang et al., 2016). A model for the methanol-based solvent exchange mechanism is proposed in Fig. 7. It is important to point out that the partial miscibility of methanol in oil enables a successful nanofiber dispersion (Zhou et al., 2006). Moreover, its largest volatility compared to water facilitates the solvent removal by vacuum rotavaporation. Thereby, methanol-based solvent exchange yields stabilized CNFs in castor oil through H-bonding of the cellulose with the hydroxyl groups present in the ricinoleic fatty acid.

3.3. *An insight into the microstructure of the cellulose nanofibers-based oleogels*

Scanning electronic microscopy enabled the visualization of the CNFs in the gel-like dispersions. Fig. 8 presents micrographs, at room temperature, corresponding to the original CNF-based hydrogels and

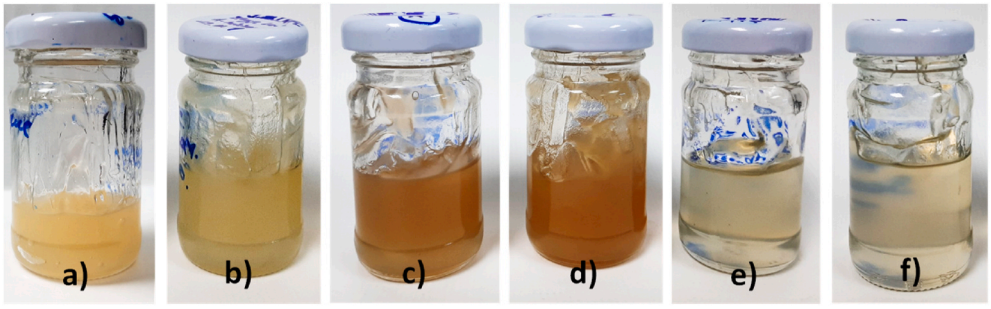

Fig. 6. Homogeneous 0.7 and 1.4 wt% oleogels successfully obtained by a methanol-based solvent exchange method: a-b) CNF–B; c-d) CNF–U; e-f) CNF-TO.

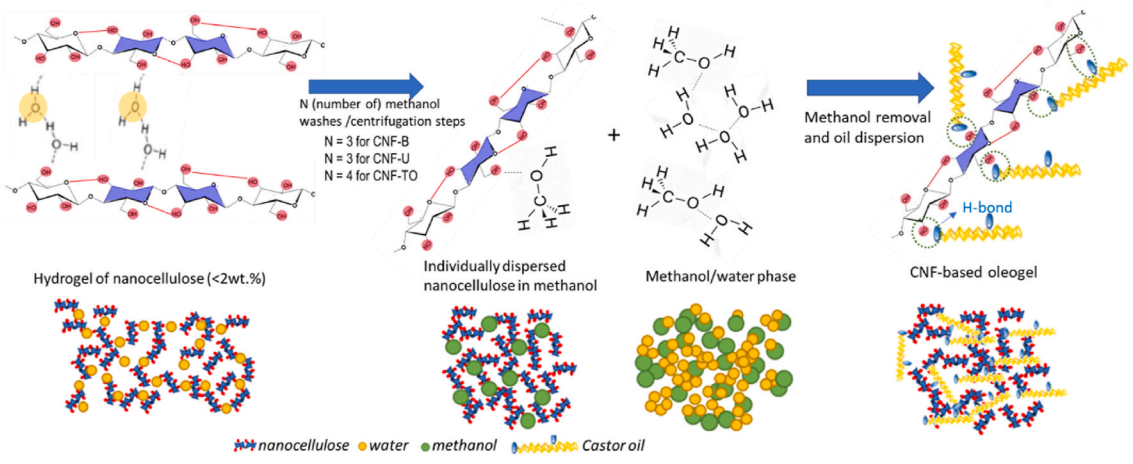

Fig. 7. Proposed model for the methanol-based solvent exchange mechanism.

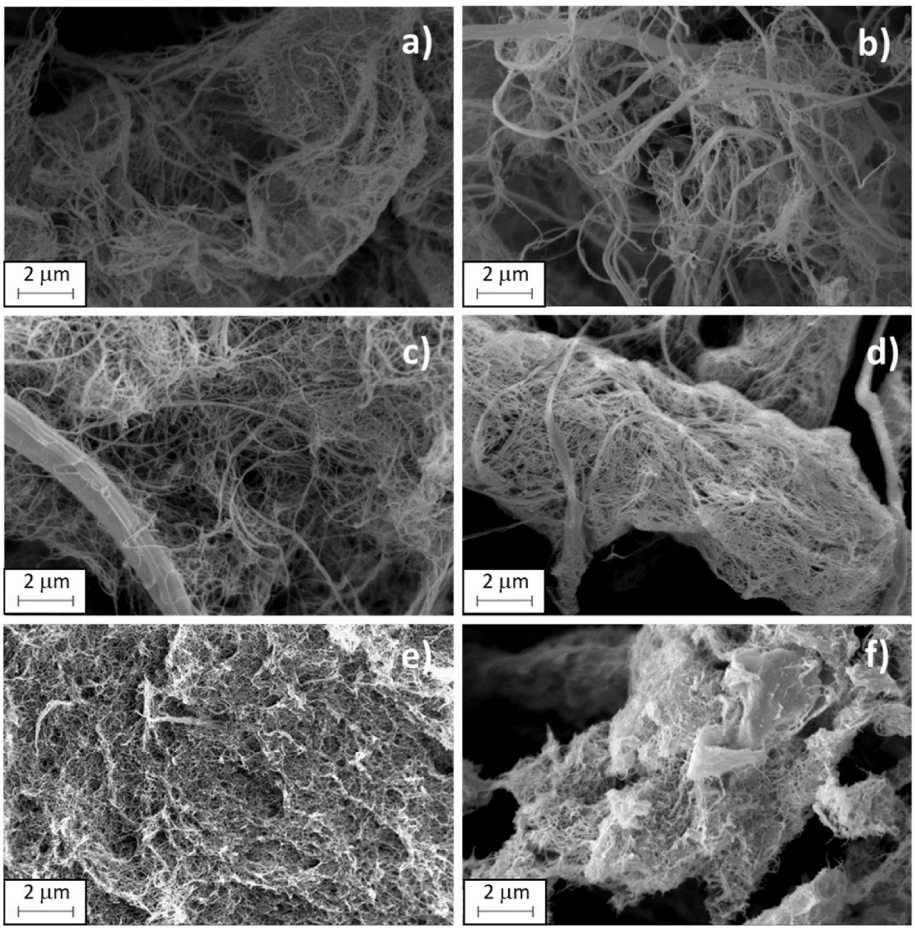

Fig. 8. SEM micrographs (7000 x) of the original CNF-based hydrogels (left column) and their corresponding 1.4 wt% CNF-based oleogels (right column): a-b) CNF–B; c-d) CNF–U; and e-f) CNF-TO.

their corresponding 1.4 wt% CNF-based oleogels. As far as the nano length scale is concerned, both CNFs obtained by mechanical treatment, i.e., CNF–B and CNF–U, gave rise to hydrogels with very similar morphologies, consisting in nanofibers with quite regular thicknesses and with varying lengths (Jimenez et al., 2020). Moreover, a significant percentage of non-fibrillated and partially fibrillated fibrils was observed, due to their fibrillation yields were 60.8 and 50.2% for CNF–B and CNF–U, respectively. Thus, at the micro length scale, these two hydrogels seem to be constituted by an entangled network of fibers with very large aspect ratios. It is worth pointing out that the micrographs in Fig. 8a to d do not indicate any distinct morphological differences between the hydrogels and their corresponding oleogels, thereby confirming that, in these cases, the methanol-based solvent exchange method proposed did not provoke cellulose fibers agglomeration. On the contrary, the TEMPO-oxidized CNF hydrogel showed a structural skeleton which consisted of well allocated and more homogeneous (100% fibrillation yield) cellulose nanofibers. Its dispersed phase is characterized by denser arrangements of much shorter and thinner fibrils than CNFs obtained by mechanical treatment (PFI refining). A part of the nanofibers seems to have agglomerated upon forming the oleogel.

In all cases, the microstructure of these 1.4 wt% CNF-based oleogels reminds that corresponding to a traditional lubricating grease, based on a soap skeleton of densely packed long and twisted fibers (Delgado et al., 2016) which may account for up to 14 wt% or even more. The oleogels studied, have much lower weight percentage of particulate phase. Even so, their skeletons also appear to be constituted by entanglements of individual fibrils or by dense fibrils arrangements. Thus, Fig. 8 demonstrates the potential of the methanol-based solvent exchange method for assisting the transferring of the CNFs from the hydrogel to the oil with, in general, no evidence for the nanofibers compaction. The observed microstructures support the outstanding thickening capacity of cellulose nanofibers in castor oil, even at very low weight concentrations, and explain the bulk rheological properties later described.

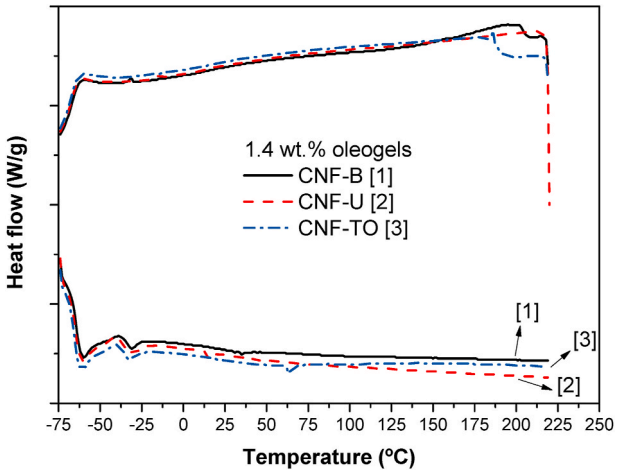

Fig. 9. DSC analysis on 1.4 wt% CNF-based oleogels.

3.4. On the oleogels' thermal analysis

Fig. 9 shows the DSC thermal characterization of 1.4 wt% CNF-based

Table 3
Consistency and oxidation onset temperature of the cellulose nanofiber-based oleogels studied.

OLEOGELS	UNWORKED PENETRATION (dmm)// NLGI GRADE[i]	*OOT* (ASTM E2009–08) (°C)
CASTOR OIL	–	198.00 ± 3.00
0.7 WT.% CNF–B	>500/000	189.02 ± 5.84
0.7 WT.% CNF–U	>500/000	193.69 ± 7.51
0.7 WT.% CNF-TO	>500/000	215.86 ± 1.32
1.4 WT.% CNF–B	449/000	189.34 ± 0.09
1.4 WT.% CNF–U	408/00	183.16 ± 0.19
1.4 WT.% CNF-TO	469/000	214.11 ± 0.12

[i] It is an approximation of NLGI grade based on the one-quarter-scale penetration values according to ASTM D217.

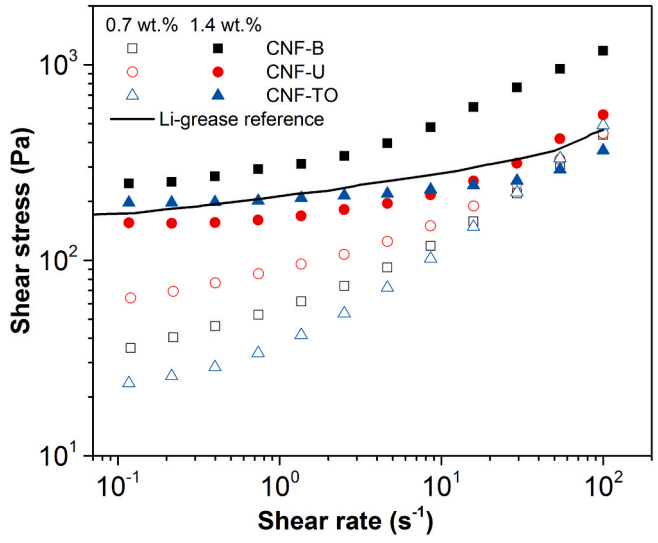

Fig. 10. Steady state viscous flow behavior, at 25 °C, for the three types of NCF-based oleogels studied, at 0.7 and 1.4 wt% (a lithium-based lubricating grease has been included as reference).

oleogels. In general, the CNF-based oleogels studied showed an excellent thermal stability within a wide temperature range (−50 to 200 °C). In contrast to the traditional lubricating greases, which display a well-defined peak corresponding to the melting of the metallic soap used as thickener (grease's skeleton) (Delgado et al., 2005), no thermal events were observed in the thermograms in Fig. 9. This result suggests higher dropping points (higher temperature before the skeleton collapses) as compared to traditional lubricating greases.

Furthermore, the resistance to oxidation of the cellulose nanofiber-based oleogels was quantified by the oxidation onset temperature (*OOT*) measured according to the ASTM E2009-08 standard. The test swiftly provides a relative measure of the oxidative stability of vegetable oil-based lubricants at a given heating rate and oxidative environment (Quinchia et al., 2011). The respective *OOT* values of oleogels studied are listed in Table 3. As can be appreciated, the TEMPO-oxidized cellulose nanofibers provided better oxidation resistance than non-oxidized nanofibers, regardless their concentration. This fact points out that the selective conversion of the C6 primary hydroxyl groups of cellulose to carboxylate groups delayed castor oil oxidation. Thus, castor oil *OOT* was enhanced from 198.0 to 215.0 °C, i.e., an improvement of 8.6%, by adding 0.7 wt% CNF-TO. This result demonstrates the great potential of CNF-TO as antioxidant additive in eco-lubricant formulations.

3.5. Mechanical performance of the cellulose nanofiber-based oleogels from a rheological perspective

The evolution of shear stress with shear rate for the three CNF-based oleogels studied is displayed, at 25 °C and as a function of CNFs concentration, in Fig. 10. In general, their viscous flow behavior was characterized by a first nearly constant stress region, at the lowest shear rates, followed by a monotonic increase in shear stress with shear rate, which denotes their pronounced pseudoplastic character. This viscous flow behavior is typical of yielding materials, i.e., materials which internal structure is such that a minimum shear stress needs to be applied before their elastic limit is exceeded and the material's flow commences (Delgado et al., 2019). Moreover, the viscous flow curves of 1.4 wt% oleogels passed through a minimum value before shear stress increased with shear rate. Such a behavior has been reported to correspond to a dynamically non-stable region, due most probably to a non-homogeneous field of velocities during the viscometric flow of this complex material (Britton and Callagham, 1997; Delgado et al., 2019). As it was expected, a larger nanofiber concentration yielded higher shear stress values and increased the oleogels' pseudoplastic behavior. A synthetic lithium-based lubricating grease, having a similar unworked penetration (434 dmm) as the 1.4 wt% oleogels (see Table 3), has been included in Fig. 10 for the sake of comparison. Even though the reference grease had a concentration of lithium soap-based thickener of 8 wt % (Delgado et al., 2006), the observed shear stress values and pseudoplasticity level, at 25 °C, were very similar to the 1.4 wt% oleogels herein studied. This fact reveals the outstanding capacity of CNF as both viscosity enhancer and structuring agent of vegetable oil-based lubricants.

Moreover, Fig. 11 demonstrates a strong dependence on both concentration and nanofiber type of the oleogels' linear viscoelastic behavior, at 25 °C. At the highest concentration studied of 1.4 wt%, a nearly constant value of the elastic modulus G' was observed within the frequency interval tested, whilst the viscous modulus G'' presented a clear minimum, thus demonstrating the typical rheological behavior of entangled networks (Delgado et al., 2006). This result agrees with the previously reported SEM micrographs (Fig. 8) which, at such a concentration of 1.4 wt%, demonstrated the formation of physical entanglements and dense arrangements of micro and nanofibers. In addition, the viscoelastic behavior of the 1.4 wt% oleogels, mainly those from bleached nanofibers, resembles the traditional lithium soap-based lubricating grease used as reference. Despite their lower moduli, as compared to the reference material, the oleogels presented a larger balance of the elastic response relative to the viscous response within the frequency window of study. This result suggests a highly elastic contribution of the cellulose nanofibers to the overall dynamic shear modulus $G^* = G' + i{\cdot}G''$ of the oleogels. At a smaller concentration, 0.7 wt% CNF, the onset of the glass transition zone, characterized by a notorious increase of the G' and G'' moduli with frequency, appeared at lower frequency values as compared to the 1.4 wt% oleogels. This result would denote a smaller extent of the plateau region, as expected from a lower degree of structuring.

It is interesting to point out that at 1.4 wt%, the CNF–B and CNF-TO oleogels showed larger values of shear stress and viscoelastic moduli than the CNF–U oleogel, even though the later showed higher consistency. However, at 0.7 wt% the unbleached CNF gave rise to a higher degree of internal structuring. It seems that, at low CNF concentration, a higher content of non-fibrillated or partially fibrillated fibrils (microfibrils) in the CNF–U sample significantly contributed to building up an internal skeleton which enhanced the oleogel structural stability. However, a higher nanofiber concentration such as 1.4 wt% seems to have enabled the formation of a percolated network through physical entanglements between cellulose nanofibers. Thus, the CNFs with higher nanofibrillation yield would exhibit a better rheological performance. The so-called "plateau modulus" G_N^0, taken as the average G' value at the "rubbery" region (or more specifically at the frequency

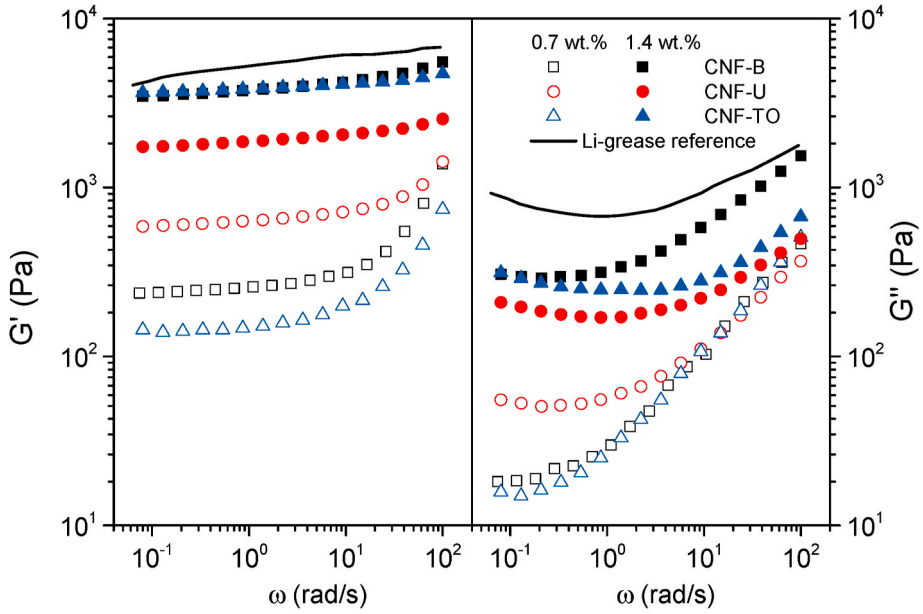

Fig. 11. Frequency dependence, at 25 °C, of the linear elastic (G′) and viscous (G'') moduli for the three types of NCF-based oleogels studied, at 0.7 and 1.4 wt% (a lithium-based lubricating grease has been included as reference).

corresponding to the $tan\delta=G''/G'$ minimum value), gives an idea on the strength of the oleogel's physically entangled structure (Delgado et al., 2006). In that sense, both the CNF–B and CNF-TO oleogels presented, at 1.4 wt%, larger values of G_N^0 than the CNF–U oleogel, thus suggesting that a larger value of shear stress has to be applied before yielding is observed (Fig. 10).

4. Conclusions

A solvent exchange strategy based on methanol enabled the production of 100% ecofriendly oleogels made up of cellulose nanofibers and castor oil. It was concluded that the methanol molecule may displace the water molecule away from the cellulose nanofibers. Thus, methanol partial miscibility in vegetable oil favors CNFs dispersion. It facilitates the CNFs stabilization in castor oil by H-bonding with the ricinoleic fatty acid when the solvent is completely removed. Three types of cellulose nanofibrils from elm cellulosic pulps were examined. A much higher water uptake was observed for CNF-TO as compared to CNF–B and CNF–U (62% vs. 28–31%, at 95% RH), which forced to increase the number of methanol wash to reach a stable oleogel. The reason behind this result is twofold. First, CNF-TO showed a stronger water affinity due to a much larger carboxylate content (1178 μmol/g vs. 53–56 μmol/g) formed by oxidation of the C6 primary hydroxyl group of cellulose molecule. And second, its higher nanofibrillation yield (100% vs. 61-50%) provided a higher surface area compared to the non-oxidized nanofibers.

Even at a concentration as low as 1.4 wt%, all CNF studied demonstrated a high thickening capacity in castor oil, yielding homogeneous and storage stable oleogels with rheological behaviors similar to a commercial lithium-based lubricating grease with comparable NLGI consistency. As shown by SEM micrographs, at such a concentration, the nanofibers phase seems to have yielded a percolated structure of entangled nanofibers or packed arrangements, thereby enhancing very significantly the elastic contribution of the complex shear modulus, mainly those nanofibrils from bleached pulps (higher fibrillation yields). Between them, CNF-TO resulted to be of special interest in eco-lubricant formulations due to its demonstrated antioxidant capacity.

Further research is being carried out in order to elucidate the effect of temperature on the rheological and tribological behavior of these cellulose nanofiber-based oleogels in a broader concentration range. Moreover, wear tests in the mixed lubrication regime are being conducted. In that sense, both the friction coefficient and the wear scar features are being assessed and contrasted with traditional lubricating greases used as reference.

CRediT authorship contribution statement

Claudia Roman: Investigation, Data curation, Writing – original draft. **Moisés García-Morales:** Methodology, Validation, Writing – review & editing. **María E. Eugenio:** Methodology, Validation, Project administration. **David Ibarra:** Methodology, Validation. **Raquel Martín-Sampedro:** Investigation, Data curation, Writing – original draft. **Miguel A. Delgado:** Conceptualization, Supervision, Writing – review & editing, Project administration.

Declaration of competing interest

The authors declare that they have no known competing financial interests or personal relationships that could have appeared to influence the work reported in this paper.

Acknowledgements & Funding

This work is part of a Research Project sponsored by "Programa Operativo FEDER-Andalucía 2014–2020" (UHU-1255843). Also, part of this investigation is included in the Research Projects "RTI2018-096080-B-C21" and RTI2018-096080-B-C22 supported by the MCIU/AEI/FEDER/UE, and SUSTEC-CM S2018/EMT-4348 by Comunidad de Madrid. Funding for open access charge: Universidad de Huelva/CBUA. The authors gratefully acknowledge their financial support.

References

Arvidsson, R., Nguyen, D., Svanström, M., 2015. Life cycle assessment of cellulose nanofibrils production by mechanical treatment and two different pretreatment processes. Environ. Sci. Technol. 49, 6881–6890. https://doi.org/10.1021/acs.est.5b00888.

Batista da Silva, J.A., Brady Moreira, F.G., Leite dos Santos, V.M., Longo, R.L., 2011. Hydrogen bond networks in water and methanol with varying interaction strengths. Phys. Chem. Chem. Phys. 13, 593–603. https://doi.org/10.1039/C0CP01204A.

Beck, S., Bouchard, J., Berry, R., 2012. Dispersibility in water of dried nanocrystalline cellulose. Biomacromolecules 13, 1486–1494. https://doi.org/10.1021/bm300191k.

Belbekhouche, S., Bras, J., Siqueira, G., Chappey, C., Lebrun, L., Khelifi, B., Marais, S., Dufresne, A., 2011. Water sorption behavior and gas barrier properties of cellulose whiskers and microfibrils films. Carbohydr. Polym. 83, 1740–1748. https://doi.org/10.1016/j.carbpol.2010.10.036.

Benson, S.P., Pleiss, J., 2013. Incomplete mixing versus clathrate-like structures: a molecular view on hydrophobicity in methanol-water mixtures. J. Mol. Model. 19, 3427–3436. https://doi.org/10.1007/s00894-013-1857-1. Epub 2013 May 18.

Besbes, I., Alila, S., Boufi, S., 2011. Nanofibrillated cellulose from TEMPO-oxidized eucalyptus fibres: effect of the carboxyl content. Carbohydr. Polym. 84, 975–983. https://doi.org/10.1016/j.carbpol.2010.12.052.

Borrero-López, A.M., Martín-Sampedro, R., Ibarra, D., Valencia, C., Eugenio, M.E., Franco, J.M., 2020. Evaluation of lignin-enriched side-streams from different biomass conversion processes as thickeners in bio-lubricant formulations. Int. J. Biol. Macromol. 16, 1398–1413. https://doi.org/10.1016/j.ijbiomac.2020.07.292.

Britton, M.M., Callagham, P.T., 1997. Nuclear magnetic resonance visualization of anomalous flow in cone-and-plate rheometry. J. Rheol. 41, 1365–1386. https://doi.org/10.1122/1.550846.

Cecilia, J.A., Ballesteros Plata, D., Alves Saboya, R.M., Murilo Tavares de Luna, F., Cavalcante, C.L., Rodríguez-Castellón, E., 2020. An overview of the biolubricant production process: challenges and future perspectives. Processes 8, 257. https://doi.org/10.3390/pr8030257.

Chang, H., Luo, J., Bakhtiary Davijani, A.A., Chien, A.T., Wang, P.H., Liu, H.C., Kumar, S., 2016. Individually dispersed wood-based cellulose nanocrystals. ACS Appl. Mater. Interfaces 8, 5768–5771. https://doi.org/10.1021/acsami.6b00094.

Cortés-Triviño, E., Valencia, C., Delgado, M.A., Franco, J.M., 2019. Thermo-rheological and tribological properties of novel bio-lubricating greases thickened with epoxidized lignocellulosic materials. J. Ind. Eng. Chem. 80, 626–632. https://doi.org/10.1016/j.jiec.2019.08.052.

Delgado, M.A., Franco, J.M., Valencia, C., Sánchez, M.C., Gallegos, C., 2005. Relationship among microstructure, rheology and processing of a lithium lubricating grease. Chem. Eng. Res. Des. 83, 1085–1092. https://doi.org/10.1205/cherd.04311.

Delgado, M.A., Secouard, S., Valencia, C., Franco, J.M., 2019. On the steady-state flow and yielding behaviour of lubricating greases. Fluid 4, 1–15. https://doi.org/10.3390/fluids4010006.

Delgado, M.A., Valencia, C., Sánchez, M.C., Franco, J.M., Gallegos, C., 2006. Influence of soap concentration and oil viscosity on the Rheology and microstructure of lubricating greases. Ind. Eng. Chem. Res. 45, 1902–1910. https://doi.org/10.1021/ie050826f.

El Seoud, O.A., Fidale, L.C., Ruiz, N., D'almeida, M.L.O., Frollini, E., 2008. Cellulose swelling by protic solvents: which properties of biopolymer and solvent matter? Cellulose 15, 371–392. https://doi.org/10.1007/s10570-007-9189-x.

Fillat, Ú., Wicklein, B., Martín-Sampedro, R., Ibarra, D., Ruiz-Hitzky, E., Valencia, C., Sarrión, A., Castro, E., Eugenio, M.E., 2018. Assessing cellulose nanofiber production from olive tree pruning residue. Carbohydr. Polym. 179, 252–261. https://doi.org/10.1016/j.carbpol.2017.09.072.

Foster, E.J., Moon, R.J., Agarwal, U.P., Bortner, M.J., Bras, J., Camarero-Espinosa, S., Chan, K.J., Clift, M.J.D., Cranston, E.D., Eichhorn, S.J., Fox, D.M., Hamad, W.Y., Heux, L., Jean, B., Korey, M., Nieh, W., Ong, K.J., Reid, M.S., Renneckar, S., Roberts, R., Shatkin, J.A., Simonsen, J., Stinson-Bagby, K., Wanasekara, N., Youngblood, J., 2018. Current characterization methods for cellulose nanomaterials. Chem. Soc. Rev. 8, 1–71. https://doi.org/10.1039/C6CS00895J.

Gallego, R., Arteaga, J.F., Valencia, C., Díaz, M.J., Franco, J.M., 2015. Gel-like dispersions of HMDI- Cross-Linked lignocellulosic materials in Castor oil: toward completely renewable lubricating grease formulations. ACS Sustain. Chem. Eng. 3, 2130–2141. https://doi.org/10.3303/CET1124248.

Iglesias, M.C., Shivyari, N., Norris, A., Martín-Sampedro, R., Eugenio, M.E., Lahtinen, P., Auad, M.L., Elder, T., Jiang, Z., Frazier, C.E., Peresin, M.S., 2020. The effect of residual lignin on the rheological properties of cellulose nanofibril suspensions. J. Wood Chem. Technol. 40, 370–381. https://doi.org/10.1080/02773813.2020.1828472.

Isogai, A., Saito, T., Fukuzumi, H., 2011. TEMPO-oxidized cellulose nanofibers. Nanoscale 3, 71–85. https://doi.org/10.1039/C0NR00583E.

Isogai, A., Zhou, Y., 2019. Diverse nanocelluloses prepared from TEMPO-oxidized wood cellulose fibers: nanonetworks, nanofibers, and nanocrystals. Curr. Opin. Solid State Mater. Sci. 23, 101–106. https://doi.org/10.1016/j.cossms.2019.01.001.

Jiménez-López, L., Eugenio, M.E., Ibarra, D., Darder, M., Martín, J.A., Martín-Sampedro, R., 2020. Cellulose nanofibers from a Dutch elm disease-resistant Ulmus minor clone. Polymers 12, 2450. https://doi.org/10.3390/polym12112450.

Kandhola, G., Djioleu, A., Rajan, K., Labbé, N., Sakon, J., Julie Carrier, D., Kim, J.W., 2020. Maximizing production of cellulose nanocrystals and nanofibers from pre-extracted loblolly pine kraft pulp: a response surface approach. Bioresour. Bioprocess 7, 1–16. https://doi.org/10.1186/s40643-020-00302-0.

Li, T., Chen, C., Brozena, A.H., Zhu, J.Y., Xu, L., Driemeier, C., Dai, J., Rojas, O.J., Isogai, A., Wågberg, L., Hu, L., 2021. Developing fibrillated cellulose as a sustainable technological material. Nature 590, 47–56. https://doi.org/10.1038/s41586-020-03167-7.

Mannekote, J.K., Satish, V., Kailas, K., Venkatesh, K.N., 2017. Environmentally friendly functional fluids from renewable and sustainable sources-a review. Renew. Sustain. Energy Rev. 81, 1787–1801. https://doi.org/10.1016/j.rser.2017.05.274.

Martín, J.A., Solla, A., Venturas, M., Collada, C., Domínguez, J., Miranda, E., Fuentes, P., Burón, M., Iglesias, S., Gil, L., 2015. Seven Ulmus minor clones tolerant to Ophiostoma novo-ulmi registered as forest reproductive material in Spain. iForest-Biogeosciences For 8, 172–180. https://doi.org/10.3832/ifor1224-008.

Martín-Alfonso, J.E., Núñez, N., Valencia, C., Franco, J.M., Díaz, M.J., 2011. Formulation of new biodegradable lubricating greases using ethylated cellulose pulp as thickener agent. J. Ind. Eng. Chem. 17, 818–823. https://doi.org/10.1016/j.jiec.2011.09.003.

Martín-Sampedro, R., Eugenio, M.E., Fillat, U., Martín, J.A., Aranda, P., Ruiz-Hitzky, E., Ibarra, D., Wicklein, B., 2019. Biorefinery of lignocellulosic biomass from an elm clone: production of fermentable sugars and lignin-derived biochar for energy and environmental applications. Energy Technol. 7, 277–287. https://doi.org/10.1002/ente.201800685.

Meriçer, Ç., Minelli, M., Giacinti Baschetti, M., Lindström, T., 2017. Water sorption in microfibrillated cellulose (MFC): the effect of temperature and pretreatment. Carbohydr. Polym. 1201–1212. https://doi.org/10.1016/j.carbpol.2017.07.023.

Michelin, M., Gomes, D.G., Romaní, A., Polizeli, M.L.T.M., Teixeira, J.A., 2020. Nanocellulose production: exploring the enzymatic route and residues of pulp and paper industry. Molecules 25, 3411. https://doi.org/10.3390/molecules25153411.

Mu, L., Wu, J., Matsakas, L., Chen, M., Vahidi, A., Grahn, M., Rova, U., Christakopoulos, P., Zhu, J., Shi, Y., 2018. Lignin from hardwood and softwood biomass as a lubricating additive to ethylene glycol. Molecules 23, 537. https://doi.org/10.3390/molecules23030537.

Nascimento, D.M., Nunes, Y.L., Figueirêdo, M.C.B., de Azeredo, H.M.C., Aouada, F.A., Feitosa, J.P.A., Rosa, M.F., Dufresne, A., 2018. Nanocellulose nanocomposite hydrogels: technological and environmental issues. Green Chem. 20, 2428–2448. https://doi.org/10.1039/C8GC00205C.

Nechyporchuk, O., Belgacem, M.N., Bras, J., 2016. Production of cellulose nanofibrils: a review of recent advances. Ind. Crop. Prod. 93, 2–25. https://doi.org/10.1016/j.indcrop.2016.02.016.

Núñez, N., Martín-Alfonso, J.E., Valencia, C., Sánchez, M.C., Franco, J.M., 2012. Rheology of new green lubricating grease formulations containing cellulose pulp and its methylated derivative as thickener agents. Ind. Crop. Prod. 37, 500–507. https://doi.org/10.1016/j.indcrop.2011.07.027.

Ogunniyi, D.S., 2006. Castor oil: a vital industrial raw material. Bioresour. Technol. 97, 1086–1091. https://doi.org/10.1016/j.biortech.2005.03.028.

Okita, Y., Fujisawa, S., Saito, T., Isogai, A., 2011. TEMPO-oxidized cellulose nanofibrils dispersed in organic solvents. Biomacromolecules 12, 518–522. https://doi.org/10.1021/bm101255x.

Okura, H., Wada, M., Serizawa, T., 2014. Dispersibility of HCl-treated cellulose nanocrystals with water-dispersible properties in organic solvents. Chem. Lett. 43, 601–603. https://doi.org/10.1246/cl.131181.

Quinchia, L.A., Delgado, M.A., Valencia, C., Franco, J.M., Gallegos, C., 2010. Viscosity modification of different vegetable oils with EVA copolymer for lubricant applications. Ind. Crop. Prod. 32, 607–612. https://doi.org/10.1016/j.indcrop.2010.07.011.

Quinchia, L.A., Delgado, M.A., Reddyhoff, T., Gallegos, C., Spikes, H.A., 2014. Tribological studies of potential vegetable oil-based lubricants containing environmentally friendly viscosity modifiers. Tribol. Int. 69, 110–117. https://doi.org/10.1016/j.triboint.2013.08.016.

Quinchia, L.A., Delgado, M.A., Valencia, C., Franco, J.M., Gallegos, C., 2011. Natural and synthetic antioxidant additives for improving the performance of new biolubricant formulations. J. Agric. Food Chem. 59, 12917–12924. https://doi.org/10.1021/jf2035737.

Rajinipriya, M., Nagalakshmaiah, M., Robert, M., Elkou, S., 2018. Importance of agricultural and industrial waste in the field of nanocellulose and recent industrial developments of wood based nanocellulose: a review. ACS Sustain. Chem. Eng. 6, 2807–2828. https://doi.org/10.1021/acssuschemeng.7b03437.

Rojo, E., Peresin, M.S., Sampson, W.W., Hoeger, I.C., Vartiainen, J., Laine, J., Rojas, O.J., 2015. Comprehensive elucidation of the effect of residual lignin on the physical, barrier, mechanical and surface properties of nanocellulose films. Green Chem. 17, 1853–1866. https://doi.org/10.1039/C4GC02398F.

Saito, T., Isogai, A., 2004. TEMPO-mediated oxidation of native cellulose. The effect of oxidation conditions on chemical and crystal structures of the water-insoluble fractions. Biomacromolecules 5, 1983–1989. https://doi.org/10.1021/bm0497769.

Saito, T., Nishiyama, Y., Putaux, J.L., Vignon, M., Isogai, A., 2006. Homogeneous suspensions of individualized microfibrils from TEMPO-catalyzed oxidation of native cellulose. Biomacromolecules 7, 1687–1691. https://doi.org/10.1021/bm060154s.

Sánchez, J.M., Franco, M.A., Delgado, C., Valencia, C., Gallegos, 2011. Thermal and mechanical characterization of cellulosic derivatives-based oleogels potentially applicable as bio-lubricating greases: influence of ethyl cellulose molecular weight. Carbohydr. Polym. 83, 151–158. https://doi.org/10.1016/j.carbpol.2010.07.033.

Segal, L., Creely, J.J., Martin, A.E., Conrad, C.M., 1959. An empirical method for estimating the degree of crystallinity of native cellulose using X-ray diffractometer Text. Res. J. 29, 786–794. https://doi.org/10.1177/004051755902901003.

Shinoda, R., Saito, T., Okita, Y., Isogai, A., 2012. Relationship between length and degree of polymerization of TEMPO-oxidized cellulose nanofibrils. Biomacromolecules 13, 842–849. https://doi.org/10.1021/bm2017542.

Solala, I., Iglesias, M.C., Peresin, M.S., 2020. On the potential of lignin-containing cellulose nanofibrils (LCNFs): a review on properties and applications. Cellulose 27, 1853–1877. https://doi.org/10.1007/s10570-019-02899-8.

Sönnichsen, N. Global lubricant demand 2000-2019. Accesed by https://https://www.statista.com/statistics/411616/lubricants-demand-worldwide/.

Wei, Y., Cheng, F., 2007. Effect of solvent exchange on the structure and rheological properties of cellulose in LiCl/DMAc. J. Appl. Polym. Sci. 106, 3624–3630. https://doi.org/10.1002/app.26886.

Zhou, H., Lu, H., Liang, B., 2006. Solubility of multicomponent systems in the biodiesel production by transesterification of Jatropha curcas L. oil with methanol. J. Chem. Eng. Data 51, 1130–1135. https://doi.org/10.1021/je0600294.